AKADÉMIAI KIADÓ

UNIVERSITY of DEBRECEN

International Review of Applied Sciences and Engineering

13 (2022) 2, 148–163

DOI:
10.1556/1848.2021.00326

ORIGINAL RESEARCH PAPER

CFD modeling of petcoke co-combustion in a real cement kiln: The effect of the turbulence-chemistry interaction model applied with K-ε variations

Z. Ngadi* and M.L. Lahlaouti

Laboratory: Energy, Faculty of Sciences of Tétouan, University Abdelmalek Essaadi, BP. 2121, 93002, Tetouan, Morroco

Received: June 11, 2021 • Accepted: August 20, 2021
Published online: September 27, 2021

ABSTRACT

Using alternative fuels (AF) in industry high consuming energy where fossil fuels are largely consumed may be a great solution to decrease CO_2 emission and cost production. Or, when using these alternative fuels, the combustion may be difficult to control regarding the different components of AFs compared to fossil fuels. In this case, the use of the computational fluid dynamics CFD tools is a great solution to predict the AFs combustion behavior. This paper represents a computational study of petcoke and olive pomace (OP) co-combustion in a cement rotary kiln burner, established on the commercial CFD software ANSYS FLUENT. This study presents a useful key to choose an adequate simulation model that well predicts co-combustion problems. The performance of the K-ε turbulence models varieties (standard, Realizable, and Re-Normalization Group) combined with the hybrid finite rate/eddy dissipation model and the simple eddy dissipation model for predicting the co-combustion characteristics was investigated. The particle phase solutions are obtained using the Lagrangian approach. The performance of the mentioned model was evaluated based on the mesh accuracy, convergence time, temperature shape, and important chemical elements concentration. The predicted values of species concentrations and temperature are compared to the results obtained from the real case study and available literature. The standard K-ε model combined with the hybrid finite rate/eddy dissipation model gives the best results and the lower computational resources required for the 2-D model realized.

KEYWORDS

CFD, combustion, turbulence model, turbulence-chemistry interaction model, alternative fuel

1. INTRODUCTION

In the last few years, there has been a growing interest from the cement industries in the Co-combustion of coal with alternative fuels (AF) for environmental and economic aims [1, 2]. Alternative fuels have different chemical and physical properties from fossil fuels [3]. Thus, particles of alternative fuels differ from coal in shape and size, so in their aerodynamics, heating up, and combustion mechanism. Modeling of coal/olive pomace (OP) Co-firing in cement kiln burner is a complex process that includes gas and particle phases as well as the effect of turbulence on combustion mechanism and heat transfer.

The computational fluid dynamics CFD plays an important role in modeling the combustion of pulverized coal/AF mixture in the rotary kiln burner. In recent years, several publications have appeared documenting the use of k-ε models for co-firing coal/AF. The Re-Normalisation Group (RNG) k-ε model is widely used for its ability to account for the swirl in the mean flow on turbulence. An interesting approach to this issue has been proposed by [4–6]. An immediate benefit of the realizable k-ε model (RKE) is that it more accurately predicts the spreading rate of round jets [7–9]. Standard k-ε (SKE) is popular in industrial

*Corresponding author.
E-mail: zakia.ngadi@gmail.com

flow and heat transfer simulation due to its robustness, economy, and reasonable accuracy for a wide range of turbulent flows and combustion [10–12]. Knaus et al. [13] studied the influence of mixing conditions, combustion air distribution, and kiln geometry on the combustion process within the wood heater on complete combustion, applying the k-ε, low Reynolds-number k-ε, and the Reynolds-stress turbulence model. They reported different flow field predictions using different turbulence models, whereas combustion characteristics (e.g., temperature and gas concentration) were predicted reasonably well by all models.

One of the turbulence-chemistry interaction models most used with the k-ε models is the eddy dissipation model (EDM) proposed by Magnussen and Hjertager [14]. Zhou, W. [15] and Ma, L. [16] have used the eddy dissipation model to evaluate the effect of turbulence on chemistry. But the major drawback of this approach can be observed especially under oxy-fuel combustion conditions. Most likely, this model over-predicts the temperatures and largely under-predicts the combustion products level [17]. An alternative to the EDM model is available in fluent [18], known as the finite rate/eddy dissipation model (FR/EDM). Several authors [10, 19–22] have used the (FR/EDM), to define the turbulence-chemistry interaction, for its accuracy to describe the turbulent combustion phenomena in pulverized fuel (PF) case and low computational cost compared to the eddy dissipation model.

Ariyaratne et al. [4] studied Meat and Bone Meal (MBM) combustion in rotary cement kiln compared to the coal combustion, using EDM with the RNG K-ε model, and they showed that the temperature profile given by the MBM is lower from the coal one over a 300 K. Another important conclusion is that the largest MBM particles are not subject to devolatilization or char burning, also MBM particle's combustion needs more oxygen mole fraction. This observation was the subject of another paper [23], whether the MBM particle size effect on combustion parameters was investigated. For modeling combustion, the FR/EDM was used for turbulence-chemistry interaction and the RNG k-ε model for turbulent flow simulation. Several publications have appeared in recent years that prove the problem of co-firing coal with AF, such as the large particle sizes, the irregularity in shapes, or either the chemical and physical properties [24–27]. The focus of this research has been on AF combustion flaws, (e.g. the pollution effect, the temperature needed, the combustion residues impact. . .). The high rotary cement kiln temperature and the intrinsic ability for clinker to absorb and lock contaminants, allow the kiln to manage most of the AF combustion problems and also burn a wide range of alternative fuels.

Although much work has been done on AF co-combustion, the authors indicated that more investigations are necessary to improve the accuracy of calculations. Furthermore, from the literature review, it is clear that there is a lack of co-firing numerical investigations concerning the cement rotary kiln. Even though the efficiency of different k-ε models with the turbulence-chemistry approach has been improved in recent years on predicting PF combustion, most improvements have been achieved by minimizing the calculation cost. Nonetheless, it is possible to further improve the efficiency by comparing these sub-models to choose the well-predicting model for novel alternative fuel. With this goal, this work seeks to develop a comparison between the three k-ε models combining with eddy dissipation model variances, in a 2D modeling case of co-firing coal with olive pomace, under rotary cement kiln burner conditions. The object is to explore the possibility of having a model that could predict well the combustion of a solid fuels mixture behavior in the kiln environment, could also take into account the difference in chemical and physical properties of AF versus coal, and could be able to give an overview of the kiln process parameters when changing the co-firing rate. In the previous work [28], we have examined the key issues in the flow field, mainly on how they are affected by turbulence models and co-processing conditions. The results obtained will be a guideline to well interpreted results obtained in this work.

The remainder of the paper is organized as follows: 1. The proposed mathematical models are presented in section 2. The computational methodology is discussed in section 3. Section 4 shows the results of different cases. Finally, section 5 concludes with a summary.

2. MATHEMATICAL MODELS

The time-averaged steady-state Navier–Stokes equations, as well as the mass and energy conservation equations are solved. The governing equations for the conservations of mass, momentum, energy, and species are the same as given in the previous work [28].

2.1. Turbulence closure models

The turbulent viscosity μ_t can be calculated with different methods [29]. For the k-ε model and its variants the turbulent viscosity is calculated as $\mu_t = C_\mu \rho k^2/\varepsilon$ where k is the turbulent kinetic energy and ε is its dissipation rate. They are obtained by solving two coupled transport equations, that have different forms according to the implemented model as detailed in the following subsections.

- Standard k-ε Model

The standard k-ε model is one of the most popular economic models in terms of accuracy. It was presented first by Jones-Launder [30], with the empirical constants given by Launder and Sharma [31]. The k and ε transport equations are presented by Eq. (1) and (2).

$$\frac{\partial}{\partial x_j}(\rho k u_j) = \frac{\partial}{\partial x_j}\left[\left(\mu + \frac{\mu_t}{\sigma_k}\right)\left(\frac{\partial k}{\partial x_j}\right)\right] + P_k - \rho\varepsilon \quad (1)$$

$$\frac{\partial}{\partial x_j}(\rho \varepsilon u_j) = \frac{\partial}{\partial x_j}\left[\left(\mu + \frac{\mu_t}{\sigma_\varepsilon}\right)\left(\frac{\partial \varepsilon}{\partial x_j}\right)\right] + C_{1\varepsilon}\frac{\varepsilon}{k}P_k - \rho C_{2\varepsilon}\frac{\varepsilon^2}{k} \quad (2)$$

In Eq. (1) and (2), P_k is the rate of turbulent kinetic energy production, and is calculated by Eq. (3),

$$P_k \approx \mu_t \left(\frac{\partial u_i}{\partial x_j} + \frac{\partial u_j}{\partial x_i}\right) \frac{\partial u_i}{\partial x_j} \tag{3}$$

- Re-normalization Group (RNG) k-ε Model

This model is derived from the instantaneous Navier-stokes equations, using a mathematical technique called renormalization group methods [32]. The k equation has the same form in Eq. (1) but ε has additional constant and term as described in Eq. (4). The additional term R_ε is given by Eq. (4), where $\eta = S k/\varepsilon$ and S is a scalar measure of the deformation tensor [18].

$$\frac{\partial}{\partial x_j}(\rho \varepsilon u_j) = \frac{\partial}{\partial x_j}\left[\left(\mu + \frac{\mu_t}{\sigma_\varepsilon}\right)\left(\frac{\partial \varepsilon}{\partial x_j}\right)\right] + C_{1\varepsilon}\frac{\varepsilon}{k}P_k - \rho C_{2\varepsilon}\frac{\varepsilon^2}{k} - R_\varepsilon \tag{4}$$

$$R_\varepsilon = \frac{C_\mu \rho \eta^3 \left(1 - \eta/\eta_0\right)}{1 + \beta \eta^3} \frac{\varepsilon^2}{k} \tag{5}$$

- Realizable k-ε Model

This model was developed [33] using a new turbulent viscosity formulation where C_μ, in the turbulent viscosity equation, it is no longer a constant but a function of the turbulent fields, mean strain, and rotation rates as described in Eq. (5). The k equation is the same as that is standard and the RNG k-ε model, contrariwise the ε equation is quite different from the other two models as specified in Eq. (7).

$$C_\mu = \frac{1}{A_0 + A_s \frac{kU^*}{\varepsilon}} \tag{6}$$

$$\frac{\partial}{\partial x_j}(\rho \varepsilon u_j) = \frac{\partial}{\partial x_j}\left[\left(\mu + \frac{\mu_t}{\sigma_\varepsilon}\right)\left(\frac{\partial \varepsilon}{\partial x_j}\right)\right] + \rho C_1 S \varepsilon - \rho C_2 \frac{\varepsilon^2}{k + \sqrt{\nu \varepsilon}} \tag{7}$$

In Eq. (6) $U^* = \sqrt{S_{ij}S_{ij} + \Omega_{ij}\Omega_{ij}}$ with $\Omega_{ij} = \frac{1}{2}\left(\frac{\partial u_i}{\partial x_j} - \frac{\partial u_j}{\partial x_i}\right)$ is the rate of rotation tensor, $A_s = \sqrt{6}\cos\phi$, $\phi = \frac{1}{3}\cos^{-1}(\sqrt{6}\,W)$ and $W = \frac{S_{ij}S_{jk}S_{ki}}{S^3}$.

In Eq. (7) the constant $C_1 = \max\left(0.43, \frac{\eta}{\eta+5}\right)$, η is the same as that in the RNG k-ε model.

The other constant in the three k-ε models are the closure coefficients and are presented in Table 1.

2.2. Turbulence-chemistry interaction models

Pulverized fuel combustion process occurs in a highly turbulent environment when the fluctuations have an important effect on the source term R_i of the species equation [28]. To this aim, the interaction between turbulent flow and reaction chemistry must be modeled with accuracy.

Generally, in co-firing coal with alternative fuels, the volatile matter can be presented by $C_xH_yO_zN_tS_n$, the values of x, y, z, t and n can be obtained from the approximate and ultimate analyses of each fuel, see Table 2. This volatile matter is considered reacting according to the simplified two-step mechanism with the intermediate species Carbon Monoxide CO, as summarized in Table 3 for coal and olive pomace. In this work, we use the eddy dissipation model (EDM) and its modified version finite rate/eddy dissipation model (FR/EDM), to calculate the coal-volatile and OP-volatile combustion.

- Eddy dissipation model (EDM)

The EDM model is based on the work of Magnussen and Hjertager [14], where R_i is directly related to the time required to mix reactants at the molecular level k/ε since the fuel consumption rate is solely determined by the turbulent mixing rate of reactant according to the work of Spalding [35]. The rate of production of species i due to the reaction, $R_{i,r}$, is given by the smaller rate of product and reactant Eq. (8), i.e., the rate that limiting the effect of the mixing process.

Table 2. Alternative and fossil fuels properties as received basis

Fuel properties	Petcock	Olive pomace
	Ultimate Analysis (wt. %)	
Carbon	88.6	51.6
Hydrogen	3.74	6
Oxygen	1.4	33.7
Sulfur	3.98	0.35
Nitrogen	1.62	1.89
	Proximate Analysis (wt. %)	
Volatile	10.6	57
Fixed carbon	87.02	16.4
Ash	0.58	4.7
Moisture	1.58	21.9
	Physical properties	
High heat value (kJ kg^{-1})	34,805	15,349
Dry particle density (kg m^{-3})	900	657
Mean particle diameter (μm)	15	200

Table 1. The three turbulence model constants

Turbulence models	Model constants
Standard k-ε	$C_{1\varepsilon} = 1.44$, $C_{2\varepsilon} = 1.92$, $C_\mu = 0.09$, $\sigma_k = 1.0$, $\sigma_\varepsilon = 1.3$ [34]
RNG k-ε	$C_{1\varepsilon} = 1.42$, $C_{2\varepsilon} = 1.68$, $C_\mu = 0.0837$, $\sigma_k = \sigma_\varepsilon \approx 1.393$ $\eta_0 = 4.38$, $\beta = 0.012$ [32]
Realizable k-ε	$C_{1\varepsilon} = 1.44$, $C_{2\varepsilon} = 1.9$, $\sigma_k = 1.0$, $\sigma_\varepsilon = 1.2$, $A_0 = 4.0$ [33]

Table 3. Global gas-phase reaction mechanism

N°	Gas-phase reaction
	Coal-volatile oxidation
1	$C_{0,78}H_{7,11}O_{0,16}N_{0,2218}S_{0,2380} + 2,32O_2 \Rightarrow 0,78CO + 3,55H_2O + 0,1109N_2 + 0,2380SO_2$
	OP-volatile oxidation
2	$C_{0,99}H_{2,27}O_{0,8}N_{0,0515}S_{0,0041} + 0,66O_2 \Rightarrow 0,99CO + 1,13H_2O + 0,0257N_2 + 0,0041SO_2$
	CO oxidation
3	$CO + 0,5O_2 \Rightarrow CO_2$

$$R_{i,r} = \nu'_{i,r} M_{w,i} A \rho \frac{\varepsilon}{k} \min\left(\min_R \frac{Y_R}{\nu'_{R,r} M_{w,R}},\ B \frac{\sum_P Y_P}{\sum_j^N \nu''_{j,r} M_{w,j}} \right) \tag{8}$$

Where R and P represent the reactants and the products index respectively. M is the molecular mass, ν is the stoichiometric coefficient and Y is the mass fraction. A and B are the mixing rate and take respectively a value of 0.4 and 5.

- *Finite rate/eddy dissipation model (FR/EDM)*

The FR/EDM model includes the rate reaction of both the finite rate and the EDM. The FR model gives the rate reaction $R'_{i,r}$ by the Arrhenius expression Eq. (9) excluding the effect of turbulence mixing. FR/EDM model chooses between the two modes based on the upcoming data from CFD simulation and, given the net reaction rate Eq. (10) as a minimum of the two models.

$$R'_{i,r} = A_r T e^{-E/RT} \tag{9}$$

$$R_i = \min\left(R_{i,r},\ R'_{i,r} \right) \tag{10}$$

Where A_r is the pre-exponential factor, E is the activation energy for the reaction, and R is the universal gas constant.

2.3. Particle phase

Alternative fuels are bigger, light in density, and have not spherical shape compared to coal, which affects the motion of particles in the furnace. In the present work, we consider AF as a spherical particle, also the AF and coal particles will be modeled separately with two discrete phases following a Rosin-Rammler size distribution [36]. The particles are tracked in Lagrangian frame reference using a stochastic model [37] as shown in Eq. (11).

$$\frac{du_p}{dt} = \frac{3\rho C_D}{4 d_p \rho_p} \left| \overline{u}_p - \overline{u} \right| \left(\overline{u} - \overline{u}_p \right) + \overline{g} \frac{\rho_p - \rho}{\rho_p} \tag{11}$$

Where $\overline{g}$ is the gravitational force, and C_D, the drag coefficient, is an empirical function of Re as described by Morsi and Alexander [38]. Here Re is the relative Reynolds number, and it is written as,

$$\mathrm{Re} = \frac{\rho d_p \left| u_p - u \right|}{\mu} \tag{12}$$

In this work, the combustion of solid particles conversion is treated as heating, devolatilizing, and char burning process. When migrating through the continuous phase in the furnace, the pulverized particles incur sequences of heterogeneous reactions, creating sources for reactions in the gas phase. Proper modeling of this particle participation is an important key role in CFD combustion.

For computing volatilization, the single kinetic rate model [39] is used. It assumes that the volatilization rate is the first-order dependent on the fraction of volatile left in the particle as shown in Eq. (13).

$$-\frac{dm_p}{dt} = k_1 \left[m_p - \left(1 - f_{v,0} \right) \left(1 - f_{w,0} \right) m_{p,0} \right] \tag{13}$$

The kinetic rate constant k_1 is defined by the Arrhenius equation as $k_1 = A_1 e^{-\left(E_1 / RT_p \right)}$. The kinetic data and the parameters of the single kinetic rate model are dependent on the properties of each fuel.

Throughout the volatilization of solid particles, only heat transfer by convection contribution (Eq. 14) is considered.

$$m_p c_p \frac{dT_p}{dt} = h_1 A_p \left(T_\infty - T_p \right) \tag{14}$$

According to Baum [40], the solid particle starts char burning until the devolatilization has completed, thus limiting the oxygen diffusion in the particle surface it remains, that the surface of the particle is diffusion-limited. When the inward-diffusing oxygen reacts with CO, which is the principal product at the char particle surface, then the combustion process is kinetic controlled. To achieve this aim, the kinetic-diffusion limited model (Eq. 15) is used for char combustion modeling.

$$\frac{dm_p}{dt} = -A_p p_{ox} \frac{D_0 R_1}{D_0 + R_1} \tag{15}$$

$$D_0 = C_1 \frac{\left[\left(T_p + T_\infty \right) / 2 \right]^{0,75}}{d_p} \tag{16}$$

$$R_1 = C_2 e^{-\left(E_1 / RT_p \right)} \tag{17}$$

The same for devolatilization occurs in the char combustion only convection and heat released by reactions are computed.

$$m_p c_p \frac{dT_p}{dt} = h_1 A_p \left(T_\infty - T_p \right) - f_h \frac{dm_p}{dt} H_{reac} \tag{18}$$

The heat transfer coefficient h_1 for Eqs. (18) and (14) is calculated using the Nusselt number of Ranz and Marshall [18].

$$Nu = \frac{h_1 d_p}{k_\infty} = 2 + 0.6\mathrm{Re}^{1/2}\mathrm{Pr}^{1/3} \quad (19)$$

3. NUMERICAL COMPUTATION AND STRATEGY

The rotary kiln used in this paper is assimilated to a real kiln with 46 m in length and 3.8 m in diameter, and it is specially equipped with a multichannel burner (see Fig. 1). For calculation purposes, the multichannel burner is converted to Fig. 1 with the applied boundary conditions cited below. The velocity and temperature and fuels feed entry are the same as in the real case. For boundary conditions, we apply in all entries an inlet velocity with normal direction to boundary except for swirl entry when both normal and tangential velocity is expected. The walls are treated as adiabatic and a no-slip condition is applied [28]. More details are given in Fig. 1. The I.T in Fig. 1 is the turbulence intensity.

A mesh test independence is applied for temperature and velocity with fore mesh size (854, 3,380, 14,040, and 31,512). To optimize convergence time, we use non-uniform mesh with higher density near the burner inlet and the axis direction and coarse in all the rest of the domain. The simulation is implemented in a 2D domain with 14,040 meshes elements for all the cases studied.

3.1. Case study

As mentioned earlier, this paper discusses the effect of the different K-ε turbulence models and the interaction turbulence-chemistry models on the CFD prediction of the co-firing coal in cement rotary kiln. To this aim, six different cases were investigated and are summarized in Table 4.

Table 4. Investigated cases details

Case	Turbulence model	Turbulence chemistry interaction model	DPM model
1	SKE	EDM	ON
2		FR/ED	
3	RNG	EDM	ON
4		FR/ED	
5	RKE	EDM	ON
6		FR/ED	

4. RESULTS AND DISCUSSION

Coal combustion in the rotary kiln is often characterized by very complicated turbulent flows. Co-combustion with AF further complicates the scenario, the AF has different physical properties from the coal. When they are transported into the kiln, they require mixing to the oxidizer, cold reactants, and hot products. In this turbulent flow, there are a lot of eddies of different lengths and velocities. To this aim, a critical view in which the model can give more information on combustion characteristics (i.e., velocity field, temperature prediction, and species distribution) is presented in this section.

4.1. Temperature prediction

Figure 2(a) illustrates temperature distribution using the three k-ε varieties. From this figure, it can be seen that a

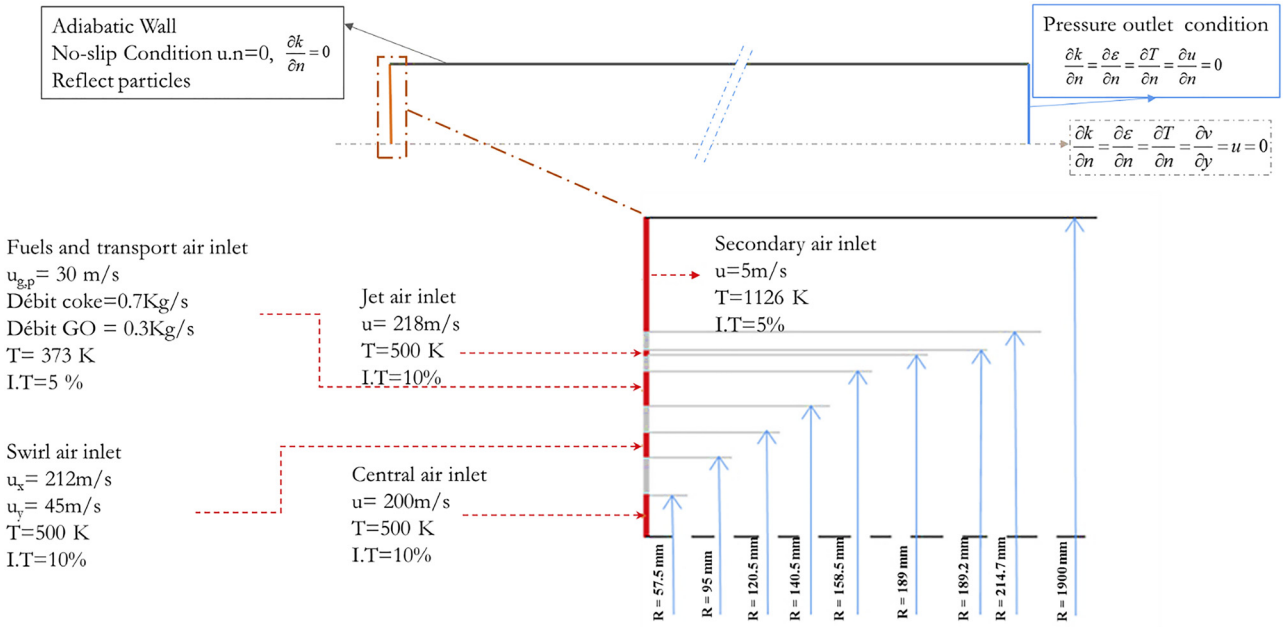

Fig. 1. Geometry and boundary conditions details

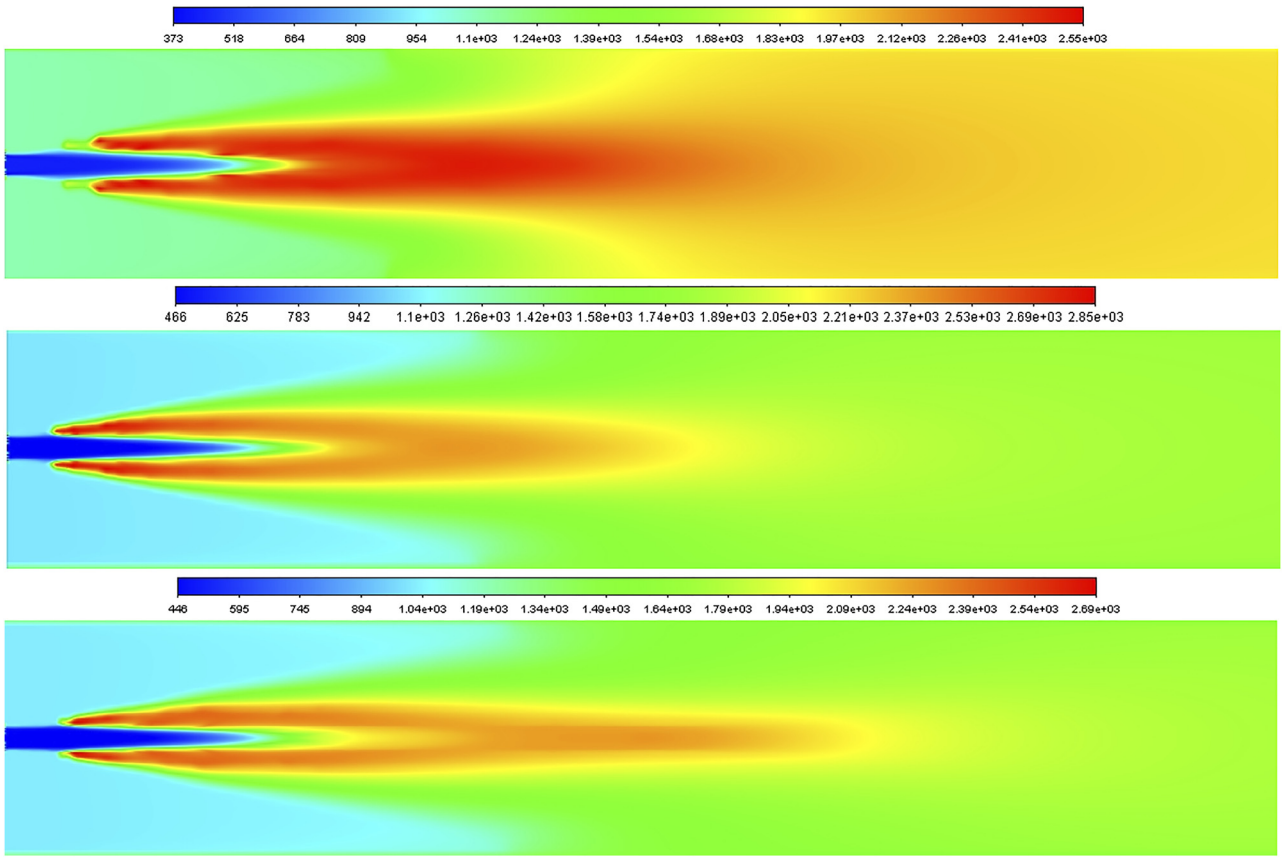

Fig. 2(a). Predicted temperature contour for the FR/ED model-based (SKE, RNG, and RKE respectively from the top)

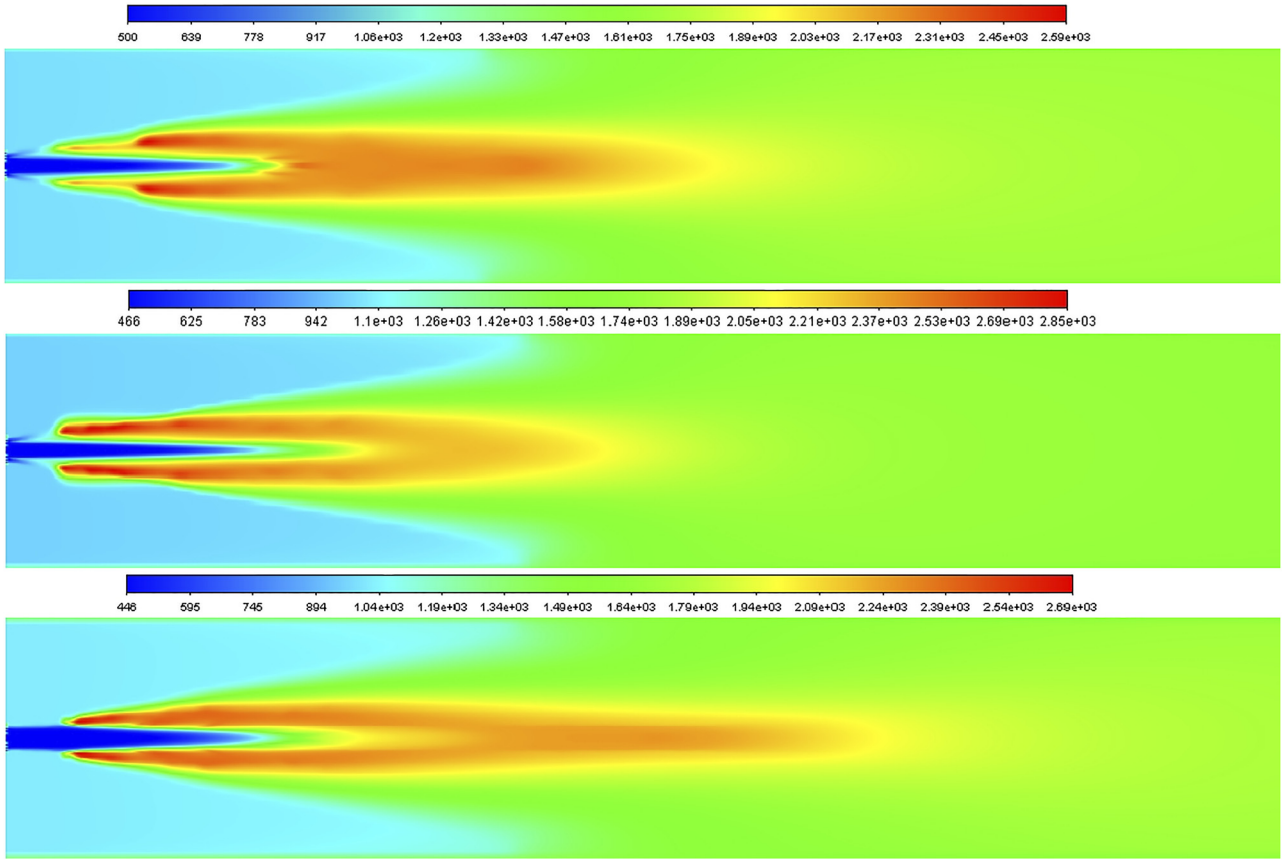

Fig. 2(b). Predicted temperature contour for the EDM model-based (SKE, RNG, and SKE respectively from the top)

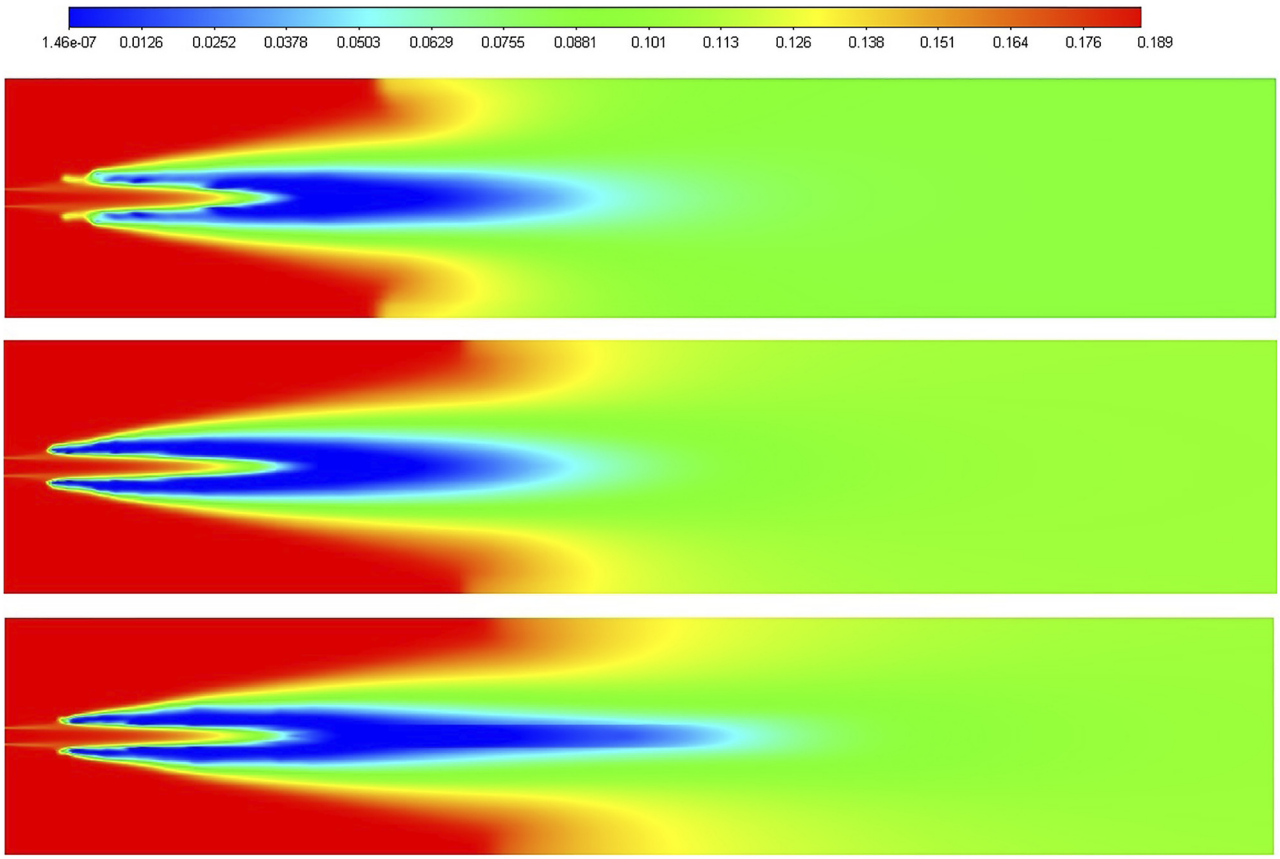

Fig. 3(a). Contour plots of oxygen mol fraction using the FR/ED model current results for (SKE, RNG, and RKE respectively from the top)

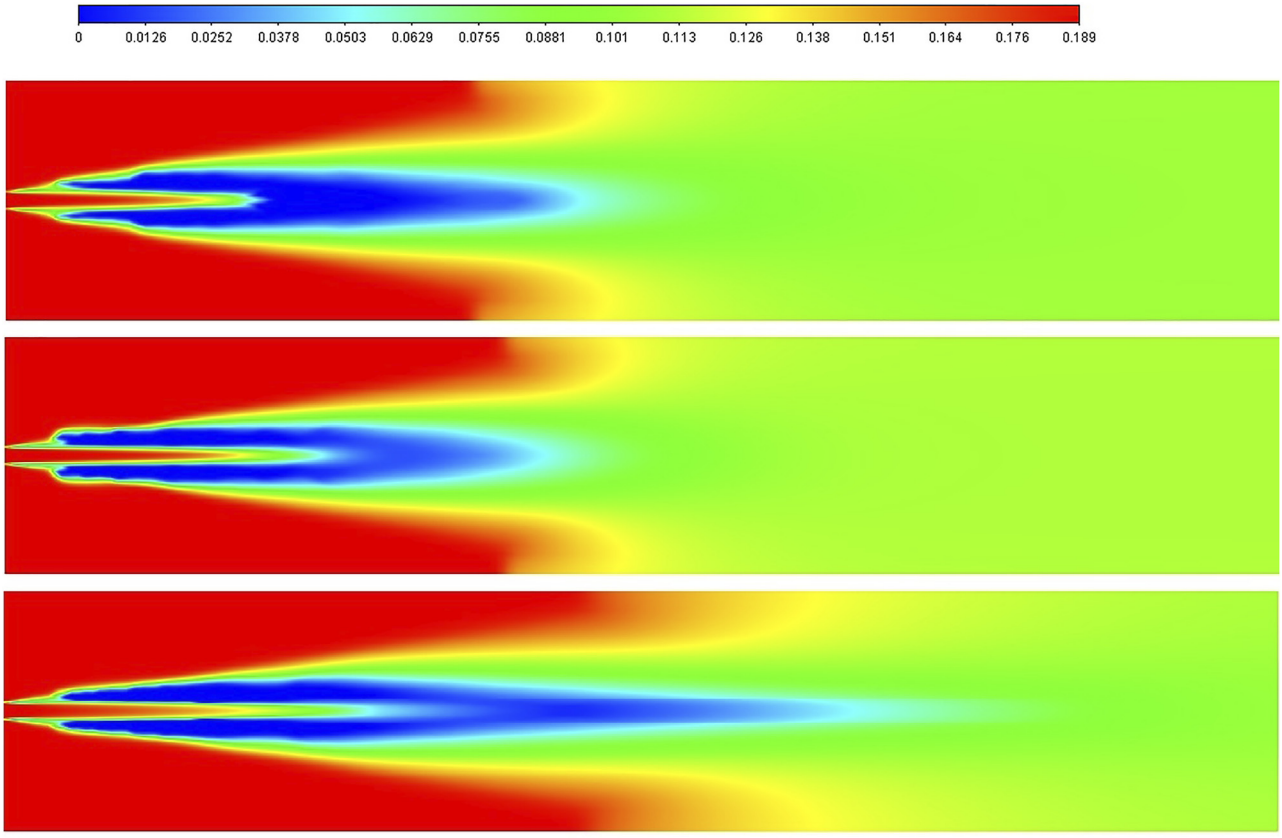

Fig. 3(b). Contour plots of oxygen mol fraction using the EDM model current results for (SKE, RNG, and RKE respectively from the top)

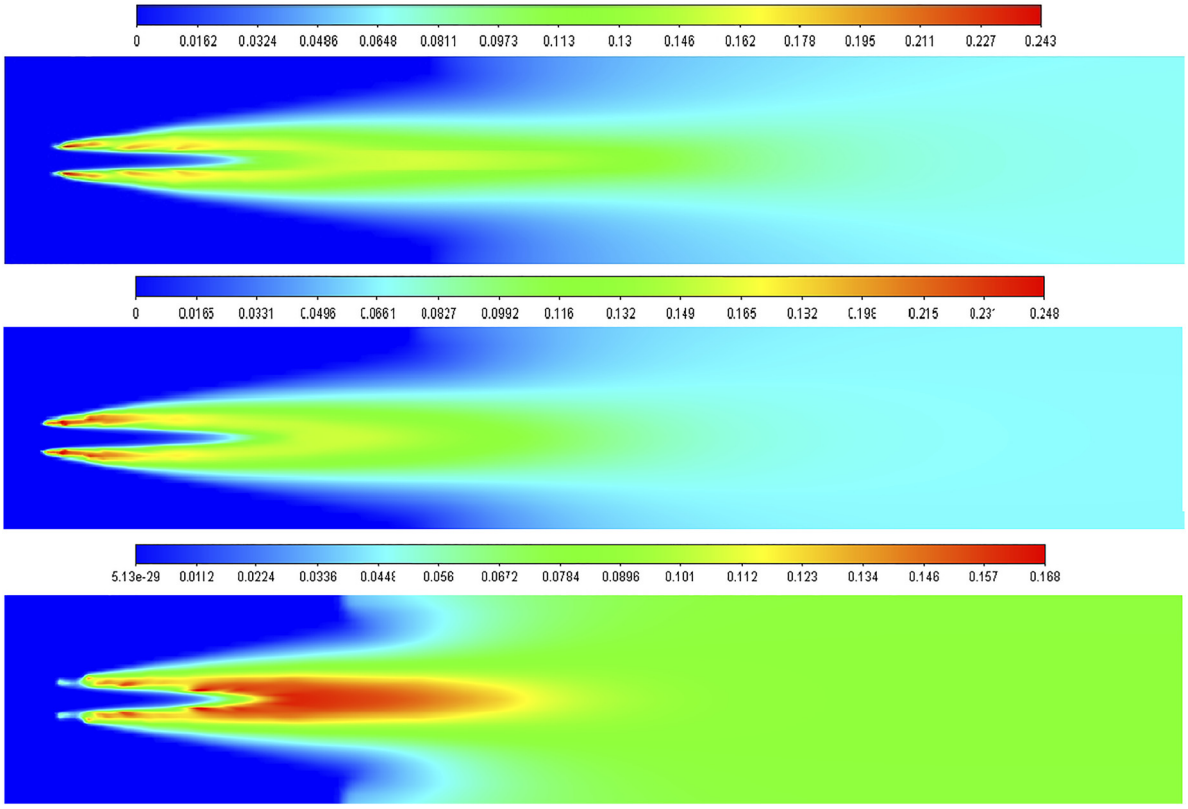

Fig. 4(a). CO_2 mole fraction contours current results for the FR/ED model cases (RKE, RNG, and SKE respectively from the top)

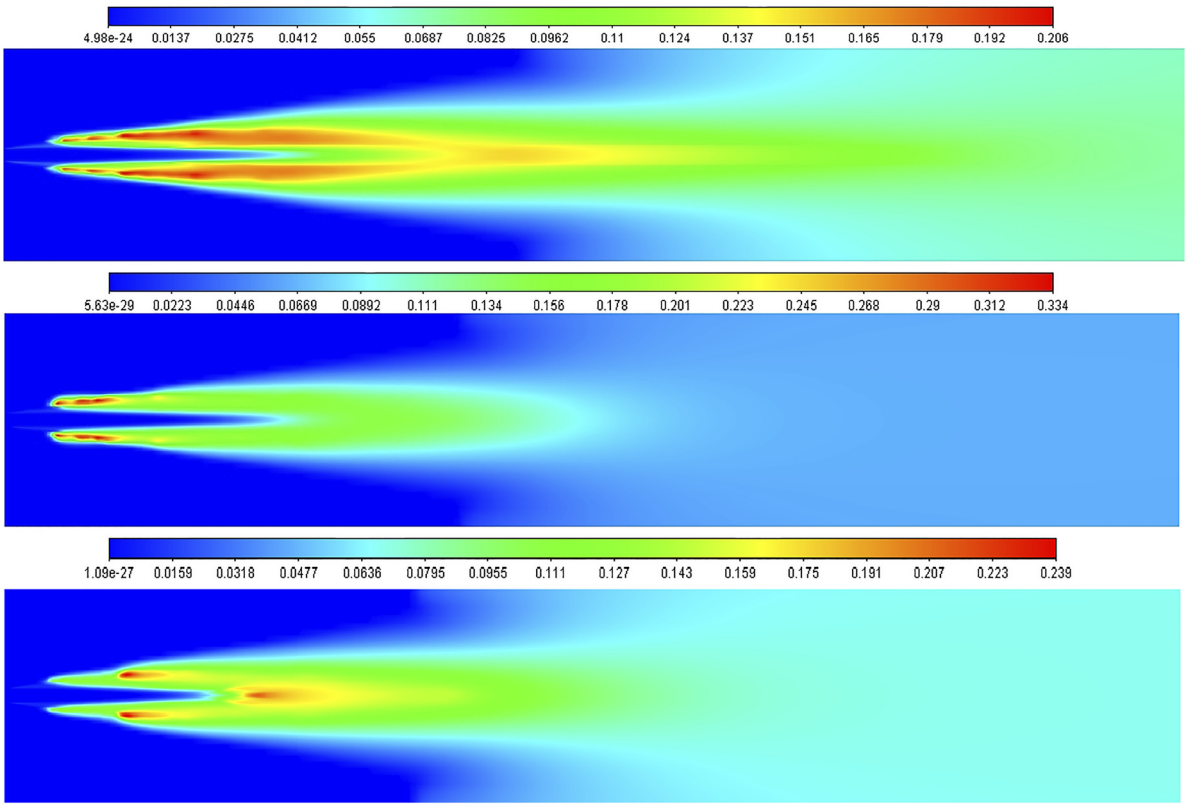

Fig. 4(b). CO_2 mole fraction contours current results for the EDM model (RKE, RNG, and SKE respectively from the top)

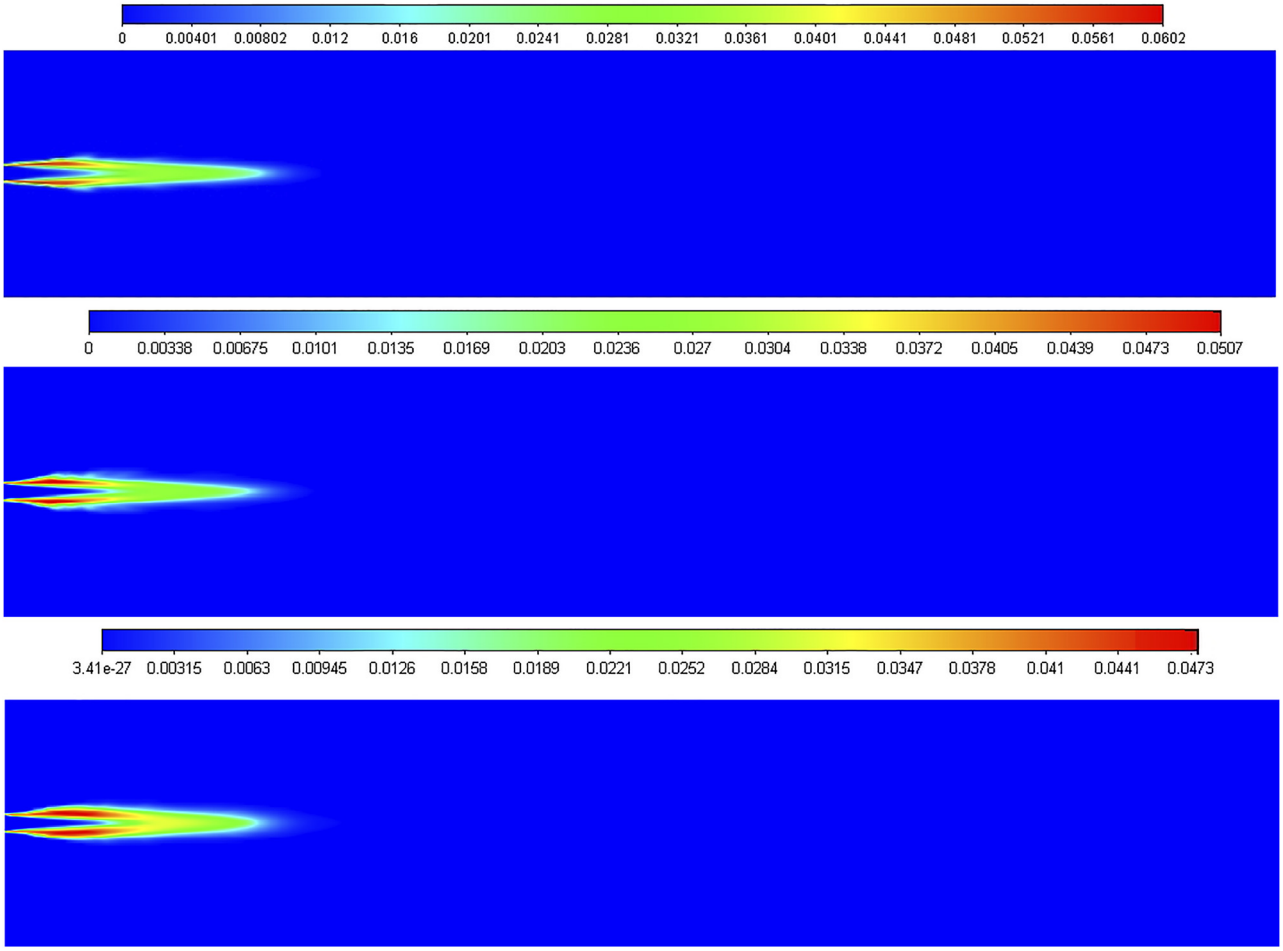

Fig. 5(a1). Predicted coal volatile mole fraction contours using the FR/ED model (RKE, RNG, and SKE respectively from the top)

low-temperature zone in front of the flame is present in the three turbulence model simulations, which cannot be seen in the real case temperature distribution as shown in Fig. 7. This is due to the drying and devolatilization of the particle model. Even though predicting different flow fields, the three k-ε models have similar trends of temperature profiles but differ in the flame length.

The RKE model gives a longer flame length because it underestimates the reverse velocity and in consequence the mixing of the cold and hot gas. In cases that use the EDM model, all models over predict the flame temperature (a pic around 2500 K) and give a longer flame, around 15 m for SKE and RNG model, as shown above in Fig. 2(b), considering the RKE model case, we remark a 25 m flame length, this is due to its dissipative nature as discussed previously, which directly impacts the EDM model production rate owing to its infinitely fast chemistry assumption. However, the simulations combined with FR/ED model perform marginally better.

For example, at 7.5 m away from the burner, all models achieve 2400 K as maximum temperature, which flows the real case, while the RKE model has a large pic temperature region as can be seen in Fig. 8.

Furthermore, along with the kiln at 12.5 m, the SKE and RNG k-ε model gives a uniform temperature 100 K lower than the kiln performs, but the RKE model still over predicting the temperature. Generally, it can be seen that the temperature profile is not affected by turbulence as much as by the turbulence-chemistry interaction models. A similar trend has been reported by several authors [41–43].

4.2. Oxygen and CO_2 fraction distribution

All simulations show low oxygen concentration near the axis and higher oxygen mass fraction in the outer region. Recalling that the fuels are injected near the burner axis thus, a low oxygen mass fraction in the axis should be expected when combustion is occurring, this will be discussed later. The influence of the turbulence model on O_2 mole fraction prediction is illustrated in Fig. 3(a). The results show that the O_2 distribution is independent of the turbulence model away from the combustion zone. Although the three turbulence models let on quite different in the low O_2 concentration zone, this is due to the variance of the predicted flow field (see [28]). Similar to the temperature contours, RKE

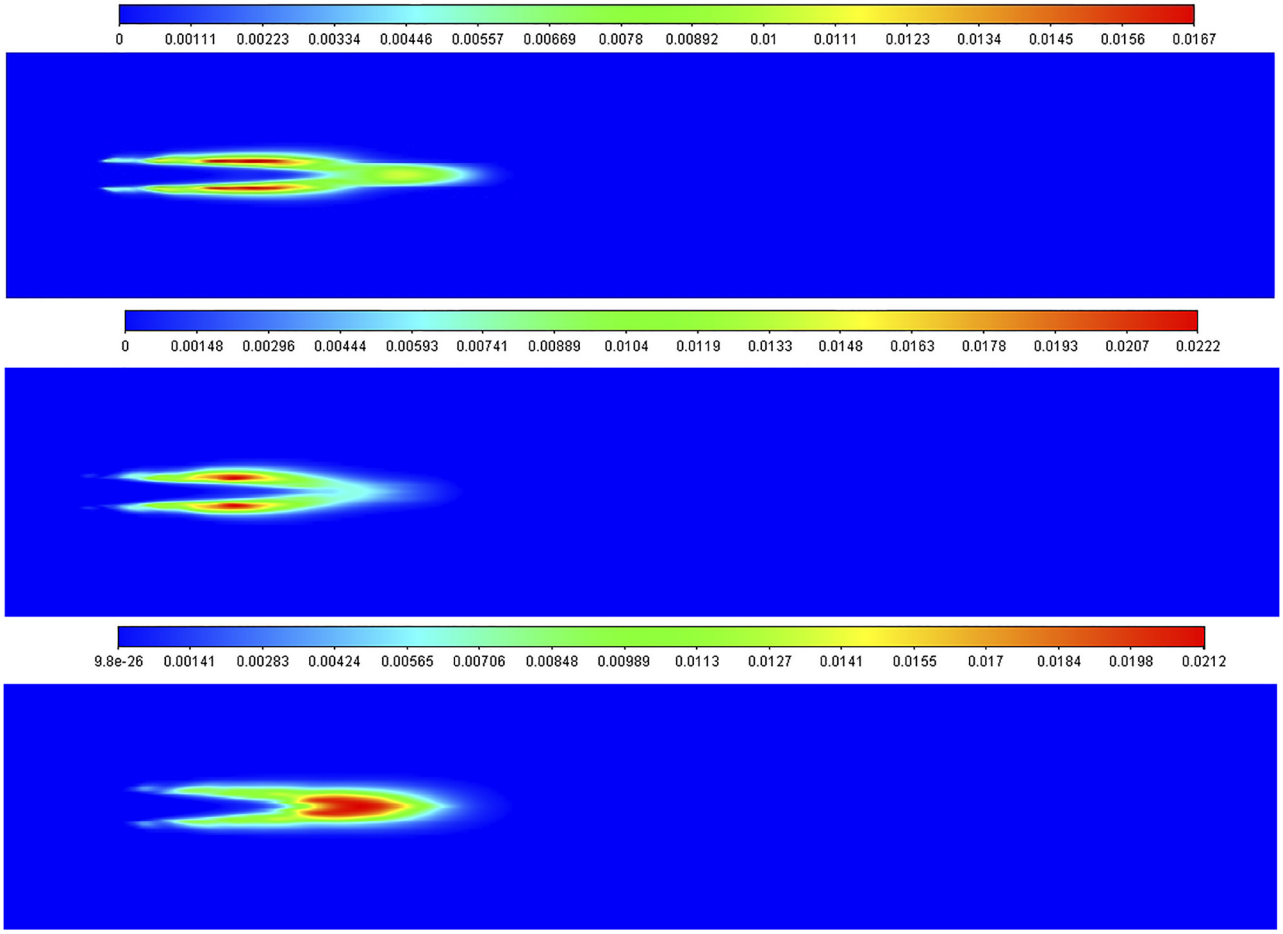

Fig. 5(a2). Predicted OP volatile mole fraction contours using the FR/ED model (RKE, RNG, and SKE respectively from the top)

provides the longer low O_2 concentration region what explains the longer flame shape obtained in this case. On the other hand, in the standard k-ε model case, a difference from the RNG model can be observed, exactly in the recirculation zone, and hence the O_2 concentration may be affected by the mixing process.

Figure 4(a) shows the comparison of the contour plot of the CO_2 mole fraction for the SKE, RNG, and RKE models. Figure 4(a) and 4(b) reveals that by adopting the different *k-ε* models, no effect on the CO_2 distribution SKE model is observed. All models give similar trends, the difference in the CO_2 concentration, due essentially to the O_2 distribution. Referring to the turbulence-chemistry interaction models, it can be observed that the whole difference is in the combustion region see Fig. 3(b). Away from this region, less formation of CO_2 and less consumption of O_2 are predicted.

Otherwise, Fig. 4(b) shows that by comparing the prediction of CO_2 between EDM and FR/ED, EDM prediction of CO_2 drops away from the flame region, this is confirming the improvement of FR/ED prediction of slow forming species. However, in the high-temperature region, the EDM model over-predicts the CO_2 concentration, this is due to its assumption to use the same model constant A and B (see Eq. 8) which may overestimate the reaction rate.

In summary, the results show that the prediction of CO_2 and O_2 is mostly independent of the turbulence model.

4.3. Volatiles and char combustion

The process of kiln destabilization has been reported in co-firing coal combustion due to the different thermodynamic and transport properties [5]. Maintaining stability and keeping the combustion of co-firing coal characteristics similar to coal combustion need special attention to volatile production near the burner, and the char combustion downstream.

Figure 5(a1) and 5(a2) show the volatile mole fraction in coal and OP mole fraction contours for FR/ED cases. Because of the fine particle size, and the high density of coal, all particles are dewatering out as soon as they are injected compared to the OP particles where the evaporation process takes place deep in the kiln. Summarizing all species distribution figures in Figs 5 and 6, it can be observed that the effect of turbulence modeling on the prediction of volatiles and CO is negligible.

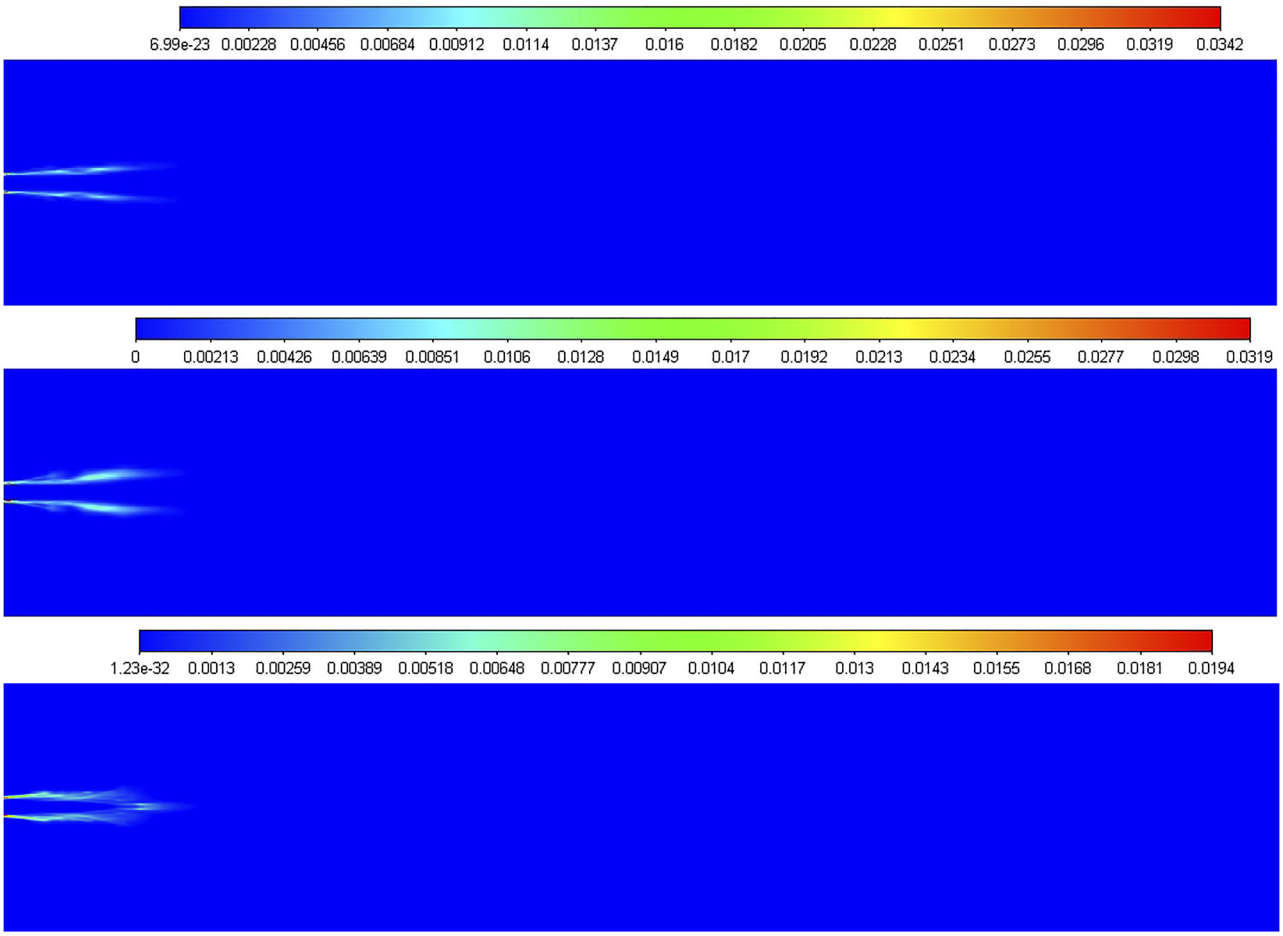

Fig. 5(b1). Predicted coal volatile mole fraction contours using the EDM model (RKE, RNG, and SKE respectively from the top)

The effect of the turbulence-chemistry interaction model on volatiles and CO production is presented in Figs 5 and 6. Figure 5(b1) and 5(b2) show that the EDM model gives faster consumption of volatile compared to the FR/ED model case, therefore, it is clear from Fig. 6(a) and 6(b) that using the EDM model high concentration of CO formation is predicted. Hence, the FR/ED model gives a longer char reaction zone, and this fits well with real case data (see Table 5) and with the O_2 and temperature prediction given with the same model.

5. COMPARISON WITH REAL DATA VALIDATION

The rotary kiln in cement industries operates at a high temperature, so the installation of equipment that can register information into the kiln is complicated. For this reason, only the external wall temperature is measured using an infrared handheld pyrometer. In this chapter, we compare the trend of the temperature simulated to the external wall real temperature.

Compared the temperature profile on the symmetry position presented in Fig. 8 to the real case profile presented in Fig. 7 we remark the same trend of temperature. The position in the real case data where the temperature is low is due to the ventilator position; this affects the kiln envelope temperature only but still gives an idea on how the temperature changes in the kiln.

It has also been remarked that the pic temperature is in the same position as in the real case when standard k-ε is used. The realizable k-ε model gives a large pic as in the real case but retarded pic is observed with the same model. Also as recommended technically the temperature with the used fuel feed the temperature must reach a range of 2100–2500 K, we remark that all the model gives approximately a temperature in the same range.

For the environmental and technical constraints, several chemical components are controlled. In the case of combustion quality control the CO and O_2 are the primordial element that gives global information on the combustion process into the kiln. In this study the CO and O_2 are measured with the differential optical absorption spectroscopy. Moreover, Table 5 summaries the CO and O_2 analysis in the combustion region in the real kiln case, it is

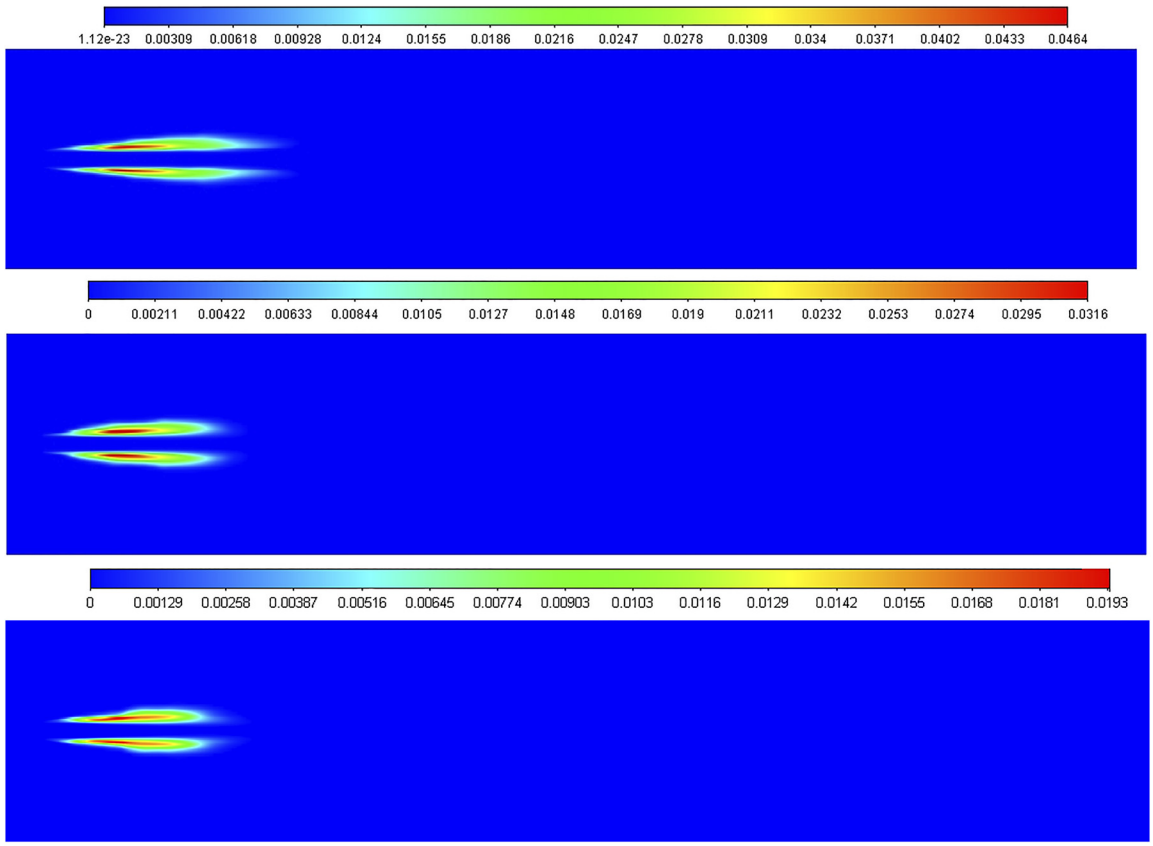

Fig. 5 (b2). Predicted OP volatile mole fraction contours using the EDM model (RKE, RNG, and SKE respectively from the top)

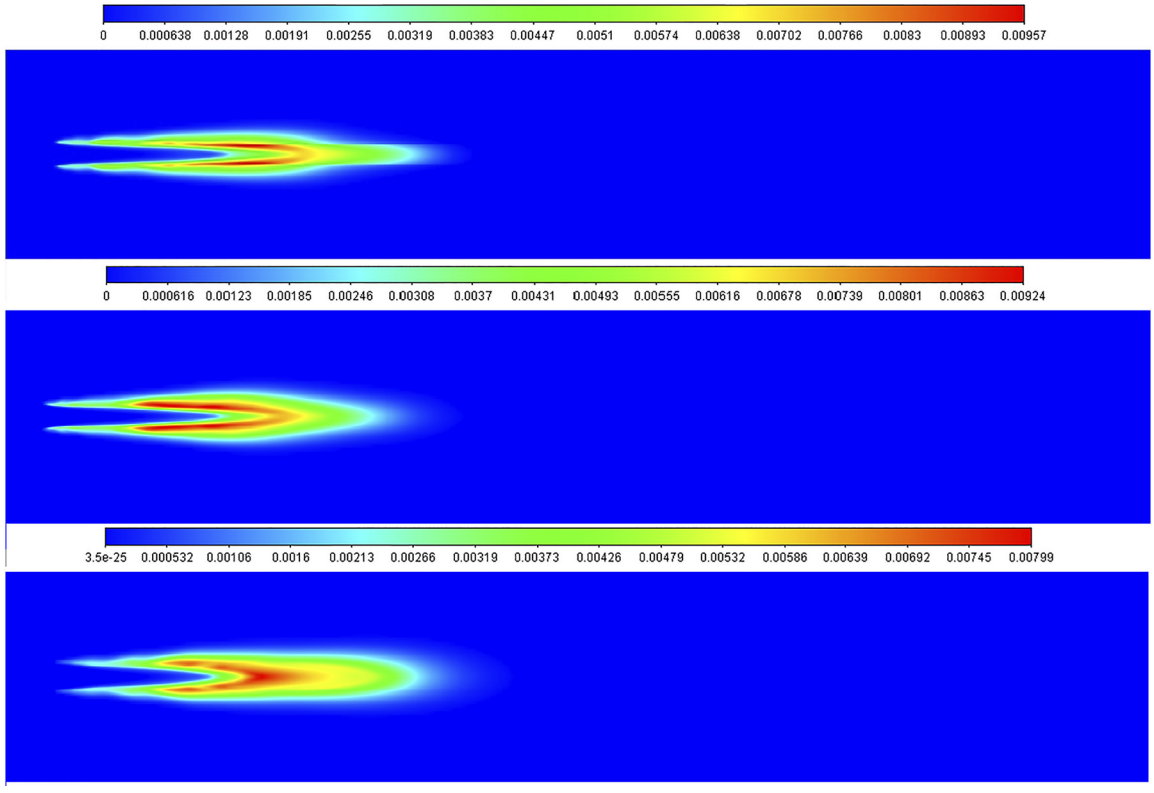

Fig. 6(a). CO mole fraction distribution predicted for the FR/ED model cases (RKE, RNG, and SKE respectively from the top)

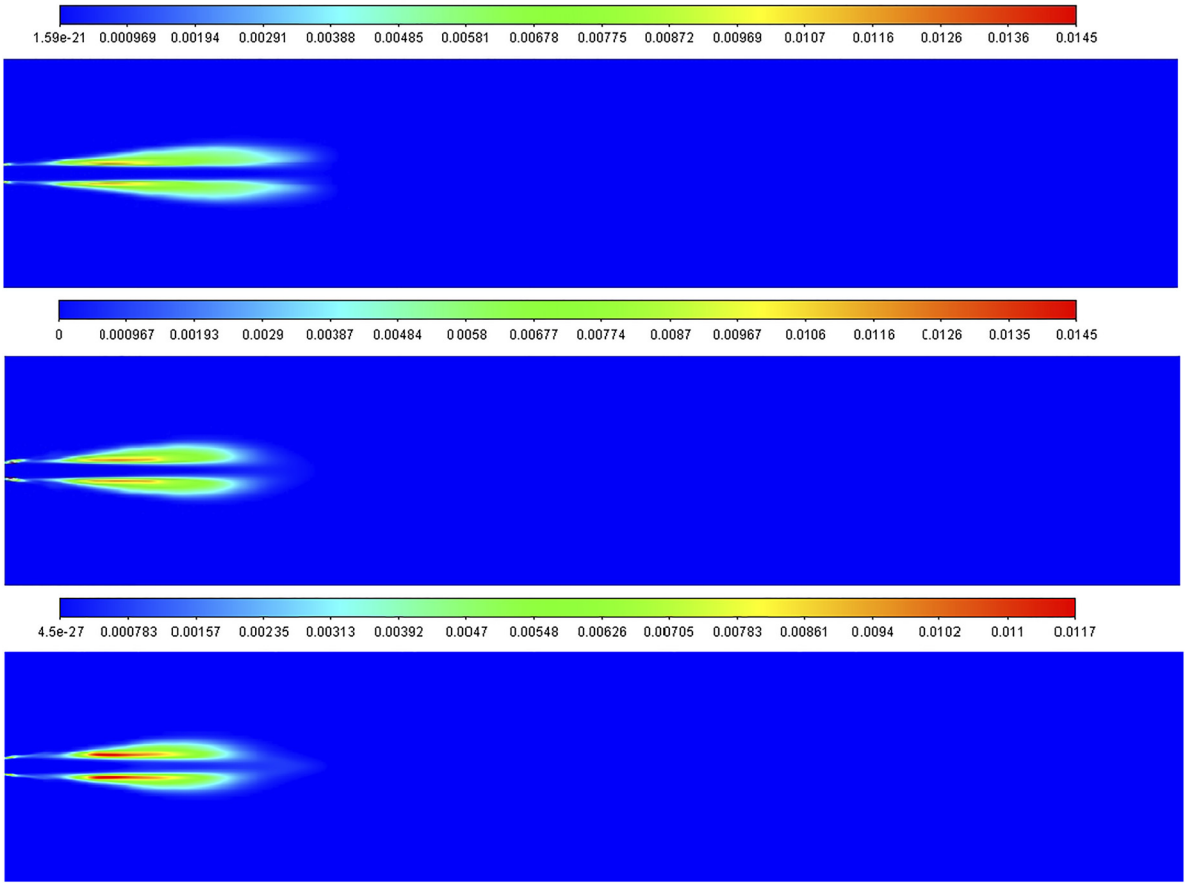

Fig. 6(b). CO mole fraction distribution predicted for the FR/ED model cases (RKE, RNG, and SKE respectively from the top)

Table 5. Species average masse fraction in the combustion region

	SKE FR/ED	RNG FR/ED	RKE FR/ED	SKE EDM	RNG EDM	RKE EDM	Real case
CO	0.00447	0.00431	0.00426	0.0068	0.0068	0.0062	0.0044
O_2	0.0159	0.0145	0.0126	0.007	0.0072	0.0061	0.017

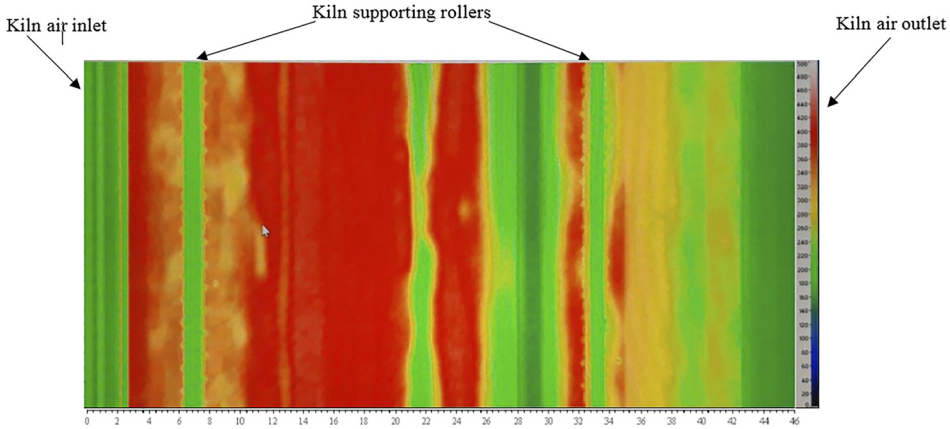

Fig. 7. Thermal profile of the real kiln wall

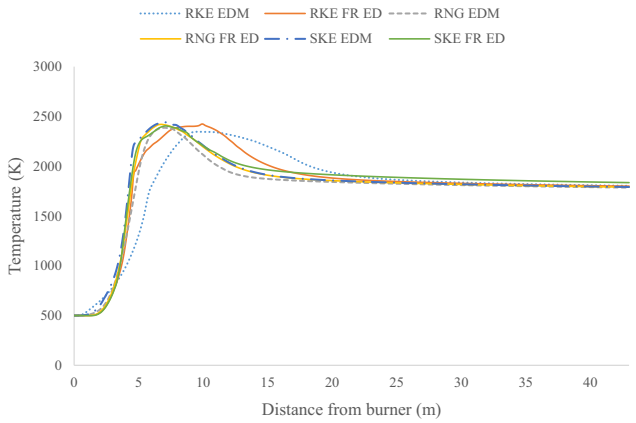

Fig. 8. Temperature profile for all K-ε models combined with the two turbulence interaction model on the symmetry position

clear that the EDM model falls in the prediction of this species, due to its based assumption, otherwise, the SKE model combined with the FR/ED model gives better agreement with the real case. Also, we remark the model that underestimated O_2 concentration is the same model that overestimates CO who confirms the good coordination of the simulation used.

6. CONCLUSION

The effect of the turbulence model (i.e., SKE, RNG, and RKE K-ε models), and the turbulence-chemistry model (i.e., the EDM model and its modification FR/ED model) on the temperature distribution, and species (i.e., O_2, CO_2, CO, and volatile) of the co-firing coal combustion gas phase of real rotary kiln case is investigated.

Six different cases are simulated and predicted, results are verified with real case data and available literature study. Based on the temperature profiles it can be seen that the temperature is not affected by turbulence as much as by the turbulence-chemistry interaction models. The main difference is observed in the flame zone and near the recirculation zone where the turbulence level is high. The same SKE model seems to fit adequately with the real kiln temperature profiles and gives the same trend of the temperature profile.

The different performance of the turbulence-chemistry model leads to different species concentration predictions, the EDM model fails to predict the O_2 concentration and over predict the CO_2 concentration which improves the good performance of the FR/ED model to predict the slow reaction species. Accordingly, while the EDM model predicts a fast consumption of volatile and high CO formation, the FR/ED model gives a longer CO reaction zone this fits well with the temperature and O_2 prediction. Generally, away from the flame zone, the level of turbulence and strain rates decay, all parameters have the same trends and keep unchangeable until the exit boundary.

On the other hand, OP conversion mechanisms, such as devolatilization and burnout are also responsible for the shift off flame from the real case, this is due to the model of volatilization, burnout, and size distribution model. Therefore, the influence of these models needs to be investigated to increase the accuracy of the simulations.

NOMENCLATURE

C_p	Heat capacity at constant pressure, J kg^{-1} K^{-1}
d_p	Current particle diameter, m
$\vec{F}$	External body force vector per unit volume, N m^{-3}
f_h	The fraction of the heat absorbed by the particle
$f_{v,0}$	Mass fraction of volatiles initially present in the particle
$f_{w,0}$	Mass fraction of the evaporating/boiling material
H_{reac}	The heat released by the surface reaction, J/Kg
h	Enthalpy, J kg^{-1}
h_1	Convective heat transfer coefficient, W/m^2k
$\vec{J_i}$	Diffusion flux of species i, kg/m^2s
m_p	Current mass of the particle, kg
$m_{p,0}$	The initial mass of the particle, kg
p_{ox}	The partial pressure of oxidant species in the gas surrounding the combusting particle, Pa
R_i	The net rate of production of species i by chemical reaction, kg/m^3s
S_i	Rate of creation of species i by addition from the dispersed phase, kg/m^3s
S_m	Mass added to the continuous phase from the dispersed second phase, kg/m^3s
Sc_t	Turbulent Schmidt number
T_p	Particle temperature, K
T_∞	The local temperature of the continuous phase, K
u	Axial velocity, m s^{-1}
$\vec{u_p}$	Particle velocity vector, m s^{-1}
μ_t	Turbulent viscosity, Pa s
ρ	The density of continuous phase, kg/m3 density of the particle, kg m^{-3}
$\bar{\bar{\tau}}$	Stress tensor, Pa

REFERENCES

[1] K. G. Kolovos, G. Kyriakopoulos, and M.S. Chalikias, "Co-evaluation of basic woodfuel types used as alternative heating sources to existing energy network," *J. Environ. Prot. Ecol.*, vol. 12, pp. 733–42, 2011.

[2] J. Koppejan, *The Handbook of Biomass Combustion and Co-firing*. 1st ed., Routledge, 2012, https://doi.org/10.4324/9781849773041.

[3] Z. Ngadi, and M.L. Lahlaouti, "Impact of using alternative fuels on cement rotary kilns: experimental study and modeling," in *Procedia Engineering*, 2017, https://doi.org/10.1016/j.proeng.2017.02.465.

[4] W.K.W.K. Hiromi Ariyaratne, A. Malagalage, M.C. Melaaen, and L. André Tokheim, "CFD modeling of meat and bone meal combustion in a rotary cement kiln," *Int. J. Model. Optimization*, vol. 4, pp. 263–72, 2014, https://doi.org/10.7763/ijmo.2014.v4.384.

[5] C. Ghenai, and I. Janajreh, "CFD analysis of the effects of co-firing biomass with coal," *Energ. Convers. Manag.*, vol. 51, pp. 1694–701, 2010, https://doi.org/10.1016/j.enconman.2009.11.045.

[6] S.R. Gubba, L. Ma, M. Pourkashanian, and A. Williams, "Influence of particle shape and internal thermal gradients of biomass particles on pulverised coal/biomass co-fired flames," *Fuel Process. Technol.*, vol. 92, pp. 2185–95, 2011, https://doi.org/10.1016/J.FUPROC.2011.07.003.

[7] C. Yin, S. Knudsen Kaer, L. Rosendahl, and S. Hvid, "Modeling of pulverized coal and biomass co-firing in a 150 KW swirling-stabilized burner and experimental validation," in *Proceedings of the International Conference on Power Engineering-09*, Japan: Kobe, 2009, https://doi.org/10.1299/jsmeicope.2009.2._2-305_.

[8] S.R. Gubba, D.B. Ingham, K.J. Larsen, L. Ma, M. Pourkashanian, H.Z. Tan, A. Williams, and H. Zhou, "Numerical modelling of the co-firing of pulverised coal and straw in a 300 MWe tangentially fired boiler," *Fuel Process. Technol.*, vol. 104, pp. 181–8, 2012, https://doi.org/10.1016/J.FUPROC.2012.05.011.

[9] S. Somwangthanaroj, and S. Fukuda, "CFD modeling of biomass grate combustion using a steady-state discrete particle model (DPM) approach," *Renew. Energ.*, vol. 148, pp. 363–73, 2020, https://doi.org/10.1016/J.RENENE.2019.10.042.

[10] A. Guessab, A. Aris, and A. Bounif, "Simulation of turbulent piloted methane non-premixed flame based on combination of finite-rate/eddy-dissipation model," *Mechanika*, vol. 19, pp. 657–64, 2013, https://doi.org/10.5755/j01.mech.19.6.6000.

[11] F. Tabet, V. Fichet, and P. Plion, "A comprehensive CFD based model for domestic biomass heating systems," *J. Energ. Inst.*, vol. 89, pp. 199–214, 2016, https://doi.org/10.1016/J.JOEI.2015.02.003.

[12] J. Chaney, H. Liu, and J. Li, "An overview of CFD modelling of small-scale fixed-bed biomass pellet boilers with preliminary results from a simplified approach," *Energ. Convers. Manag.*, vol. 63, pp. 149–56, 2012, https://doi.org/10.1016/J.ENCONMAN.2012.01.036.

[13] H. Knaus, S. Richter, S. Unterberger, U. Schnell, H. Maier, and K.R.G. Hein, "On the application of different turbulence models for the computation of fluid flow and combustion processes in small scale wood heaters," *Exp. Therm. Fluid Sci.*, vol. 21, pp. 99–108, 2000, https://doi.org/10.1016/S0894-1777(99)00059-X.

[14] B.F. Magnussen, and B.H. Hjertager, "On mathematical modeling of turbulent combustion with special emphasis on soot formation and combustion," *Symp. (International) Combustion*, vol. 16, pp. 719–29, 1977, https://doi.org/10.1016/S0082-0784(77)80366-4.

[15] W. Zhou, and D. Moyeda, "Process evaluation of oxy-fuel combustion with flue gas recycle in a conventional utility boiler," *Energy & Fuels*, vol. 24, pp. 2162–9, 2010, https://doi.org/10.1021/ef9012399.

[16] L. Ma, J.M. Jones, M. Pourkashanian, and A. Williams, "Modelling the combustion of pulverized biomass in an industrial combustion test furnace," *Fuel*, vol. 86, pp. 1959–65, 2007. https://linkinghub.elsevier.com/retrieve/pii/S0016236106005199 [accessed November 24, 2018].

[17] C. Yin, L.A. Rosendahl, and S.K. Kær, "Chemistry and radiation in oxy-fuel combustion: a computational fluid dynamics modeling study," *Fuel*, vol. 90, pp. 2519–29, 2011, https://doi.org/10.1016/j.fuel.2011.03.023.

[18] ANSYS Fluent theory guide, in: ANSYS Fluent Theory Guide 15.0. Canonsbourg, USA: Ansys,Inc, 2013, p. 193.

[19] J. Collazo, J. Porteiro, J.L. Míguez, E. Granada, and M.A. Gómez, "Numerical simulation of a small-scale biomass boiler," *Energ. Convers. Manag.*, vol. 64, pp. 87–96, 2012, https://doi.org/10.1016/J.ENCONMAN.2012.05.020.

[20] D. Djurović, S. Nemoda, B. Repić, D. Dakić, and M. Adzić, "Influence of biomass furnace volume change on flue gases burn out process," *Renew. Energ.*, vol. 76, pp. 1–6, 2015, https://doi.org/10.1016/J.RENENE.2014.11.007.

[21] Y. Bin Yang, R. Newman, V. Sharifi, J. Swithenbank, and J. Ariss, "Mathematical modelling of straw combustion in a 38 MWe power plant furnace and effect of operating conditions," *Fuel*, vol. 86, pp. 129–42, 2007, https://doi.org/10.1016/J.FUEL.2006.06.023.

[22] T. Zadravec, B. Rajh, F. Kokalj, and N. Samec, "CFD modelling of air staged combustion in a wood pellet boiler using the coupled modelling approach," *Therm. Sci. Eng. Prog.*, vol. 20, 2020, Art no. 100715, https://doi.org/10.1016/J.TSEP.2020.100715.

[23] W.K.H. Ariyaratne, A. Malagalage, M.C. Melaaen, and L.A. Tokheim, "CFD modelling of meat and bone meal combustion in a cement rotary kiln - investigation of fuel particle size and fuel feeding position impacts," *Chem. Eng. Sci.*, vol. 123, pp. 596–608, 2015, https://doi.org/10.1016/j.ces.2014.10.048.

[24] A. Panahi, M. Tarakcioglu, M. Schiemann, M. Delichatsios, and Y.A. Levendis, "On the particle sizing of torrefied biomass for co-firing with pulverized coal," *Combustion and Flame*, vol. 194, pp. 72–84, 2018, https://doi.org/10.1016/J.COMBUSTFLAME.2018.04.014.

[25] S. Seepana, S. Arumugam, K. Sivaramakrishnan, and M. Muthukrishnan, "Evaluation of feasibility of pelletized wood co-firing with high ash Indian coals," *J. Energ. Inst.*, vol. 91, pp. 1126–35, 2018, https://doi.org/10.1016/J.JOEI.2017.06.011.

[26] B.N. Madanayake, S. Gan, C. Eastwick, and H.K. Ng, "Biomass as an energy source in coal co-firing and its feasibility enhancement via pre-treatment techniques," *Fuel Process. Technol.*, vol. 159, pp. 287–305, 2017, https://doi.org/10.1016/J.FUPROC.2017.01.029.

[27] H. Mikulčić, D. Cerinski, J. Baleta, and X. Wang, "Improving pulverized coal and biomass Co-combustion in a cement rotary kiln by computational fluid dynamics," *Chem. Eng. Technol.*, vol. 42, pp. 2539–45, 2019, https://doi.org/10.1002/CEAT.201900086.

[28] Z. Ngadi, and M.L. Lahlaouti, "Coal and biomass Co-combustion: CFD prediction of velocity field for multi-channel burner in cement rotary kiln," *Proceedings*, vol. 63, p. 18, 2020, https://doi.org/10.3390/proceedings2020063018.

[29] W. Michal, "Eddy viscosity turbulence models employed by computational fluid dynamic," *Transaction Inst. Aviation*, vol. 4, pp. 92–112, 2007.

[30] W. Jones, and B. Launder, "The prediction of laminarization with a two-equation model of turbulence," *Int. J. Heat Mass Transfer*, vol. 15, pp. 301–14, 1972, https://doi.org/10.1016/0017-9310(72)90076-2.

[31] B.E. Launder, and B.I. Sharma, "Application of the energy-dissipation model of turbulence to the calculation of flow near a

spinning disc," *Lett. Heat Mass Transfer*, vol. 1, pp. 131–7, 1974, https://doi.org/10.1016/0094-4548(74)90150-7.

[32] V. Yakhot, and S.A. Orszag, "Renormalization group analysis of turbulence. I. Basic theory," *J. Scientific Comput.*, vol. 1, pp. 3–51, 1986, https://doi.org/10.1007/BF01061452.

[33] T.-H. Shih, W.W. Liou, A. Shabbir, Z. Yang, and J. Zhu, "A new k-ε eddy viscosity model for high Reynolds number turbulent flows," *Comput. Fluids*, vol. 24, pp. 227–38, 1995, https://doi.org/10.1016/0045-7930(94)00032-T.

[34] B.E. Launder, and D.B. Spalding, *Lectures in Mathematical Models of Turbulence*. London, New York: Academic Press, 1972, https://doi.org/10.1080/10256010903084126.

[35] D.B. Spalding, "Mixing and chemical reaction in steady confined turbulent flames," *Symp. (International) Combustion*, vol. 13, pp. 649–57, 1971, https://doi.org/10.1016/S0082-0784(71)80067-X.

[36] P. Rosin, and E. Rammler, "The laws governing the fineness of powdered coal," *J. Inst. Fuel*, vol. 7, pp. 29–36, 1933.

[37] J.-S. Shuen, L.-D. Chen, and G.M. Faeth, "Evaluation of a stochastic model of particle dispersion in a turbulent round jet," *AIChE J.*, vol. 29, pp. 167–70, 1983, https://doi.org/10.1002/aic.690290127.

[38] S.A. Morsi, and A.J. Alexander, "An investigation of particle trajectories in two-phase flow systems," *J. Fluid Mech.*, vol. 55, p. 193, 1972, https://doi.org/10.1017/S0022112072001806.

[39] S. Badzioch, and P.G.W.W. Hawksley, "Kinetics thermal decomposition pulverized coal particles," vol. 9, pp. 521–30, 1970, https://doi.org/10.1021/i260036a005.

[40] M.M. Baum, and P.J. Street, "Predicting the combustion behaviour of coal particles," *Combustion Sci. Technol.*, vol. 3, pp. 231–43, 1971, https://doi.org/10.1080/00102207108952290.

[41] Z.F. Tian, P.J. Witt, M.P. Schwarz, and W. Yang, "Comparison of two-equation turbulence models in simulation of a non-swirl coal flame in a pilot-scale furnace," *Combustion Sci. Technol.*, vol. 181, pp. 954–83, 2009, https://doi.org/10.1080/00102200902925679.

[42] H. Yilmaz, O. Cam, S. Tangoz, and I. Yilmaz, "Effect of different turbulence models on combustion and emission characteristics of hydrogen/air flames," *Int. J. Hydrogen Energ.*, vol. 42, pp. 25744–55, 2017, https://doi.org/10.1016/j.ijhydene.2017.04.080.

[43] L. Chen, S.Z. Yong, and A.F. Ghoniem, "Oxy-fuel combustion of pulverized coal: characterization, fundamentals, stabilization and CFD modeling," *Prog. Energ. Combustion Sci.*, vol. 38, pp. 156–214, 2012, https://doi.org/10.1016/j.pecs.2011.09.003.